Mechanisms of *p*-GaAs(100) surface by atomic force microscope nano-oxidation

2005 J. Phys. D: Appl. Phys. 38 2424

(http://iopscience.iop.org/0022-3727/38/14/019)

INSTITUTE OF PHYSICS PUBLISHING JOURNAL OF PHYSICS D: APPLIED PHYSICS

J. Phys. D: Appl. Phys. **38** (2005) 2424–2432 doi:10.1088/0022-3727/38/14/019

Mechanisms of *p*-GaAs(100) surface by atomic force microscope nano-oxidation

Sheng-Rui Jian[1], **Te-Hua Fang**[2] **and Der-San Chuu**[3]

[1] Department of Electrophysics, National Chiao Tung University, Hsinchu 300, Taiwan
[2] Department of Mechanical Engineering, Southern Taiwan University of Technology, Tainan 710, Taiwan

E-mail: dschuu@mail.nctu.edu.tw

Received 7 March 2005, in final form 10 May 2005
Published 1 July 2005
Online at stacks.iop.org/JPhysD/38/2424

Abstract

Nanopattering using atomic force microscope (AFM) has become an important area of research, for both fundamental research and future nanodevice applications. Local oxidation of *p*-GaAs(100) surface by using a negatively biased conductive AFM tip is a universal method for this purpose. The dependences of the height, aspect ratio and volume on applied anodization times and voltages during which the anodization voltage is applied were studied. We explore the kinetics and mechanisms of the anodization process and how factors such as the electric field strength and the relative humidity influence its growth rate and the contribution of ionic diffusion. The results revealed that the protruding oxide dot's height, aspect ratio and volume increase during longer anodization time and at larger anodization voltage as well as in higher relative humidity conditions. The high initial growth rate ($\sim$300 nm s^{-1} for 10 V) decreases quickly with decreasing electric field strength and the oxide practically ceases to grow at an order of (2–3)$\times 10^7$ V cm^{-1}. Auger electron spectroscopy measurements confirm that the modified structures take the form of anodized *p*-GaAs(100). Also, the contribution of ionic diffusion increases by about 80% at a higher relative humidity. In addition, the nanohardness of the oxide structures was measured with the aid of an AFM-based nanoindentation technique.

(Some figures in this article are in colour only in the electronic version)

1. Introduction

Understanding the detailed mechanisms of local surface oxidation is a crucial challenge in the field of nanoscience and nanotechnology since the dimensions of devices are now moving towards the nanometre-scale. Patterning and fabricating materials on a nanometre-scale using scanning probe microscopy (SPM) nano-oxidation has drawn wide attention in surface science investigations; the first report of tip-induced oxidation on H-passivated Si(111) surfaces was investigated by Dagata *et al* [1]. In particular, atomic force microscope (AFM) is a powerful experimental technique for nanofabrication because it can operate on insulating as well as conductive surfaces and has proved to be successful in imaging surfaces at an atomic level. That is to say, the AFM-based oxidation method provides a useful means for nanodevices and nanostructures fabrication not only on metals but also on semiconductors [2–6].

Up to now, several AFM modes (including contact [7], tapping [8] and non-contact [9]) have been applied to perform local oxidation lithography. AFM is operated in the non-contact mode (nc-AFM) to avoid damage to the surface and extend the tip's lifetime as well as to improve the fabricated resolution during the nano-oxidation process [9–11]. The tip's lifetime is greatly increased because of the absence of contact forces. The nc-AFM eliminates lateral shear forces and overcomes the tip–sample adhesion forces and capillarity and, the tip is in weak interaction with the surface. In addition, nc-AFM oxidation allows controlling the lateral dimensions and exhibits higher aspect ratio (height/width) for performing local oxidation lithography [12].

[3] Author to whom any correspondence should be addressed.

In the context of nc-AFM tip-induced nano-oxidation on a p-GaAs(100) surface, the goal of this study was twofold: first, to fabricate nanometre-scale dot structures; and second, to analyse and investigate the characteristics of the oxidation mechanisms at various anodization voltages, anodization time and relative humidity. In addition, it has become necessary to measure the hardness of materials such as with micro/nanoscale structures for micro/nanoelectromechanical applications. New techniques are needed to take measurements at very shallow depths. Mechanical and structural aspects are of critical importance in integrating nanoscale building blocks into functional micro/nanodevices; thereby, the AFM-based nanoindentation technique was applied to anodized structures to determine their nanohardness values.

2. Experimental details

In this paper, nanolithography is performed by means of a commercial AFM (CP-R SPM, Veeco/TM, USA) and lithography software for non-contact dynamic mode to perform the oxidation experiments. A Pt-coated probe with a silicon cantilever is used. The curvature radius of the tip is 35 nm. The force constant and the resonance frequency of the non-contact mode cantilevers used are 34 N m^{-1} and 350 kHz, respectively. The specimen is p-GaAs(100) with a resistivity of 10 Ω cm, with a root-mean-square surface roughness of less than 0.2 nm and an average surface roughness of less than 0.3 nm. Before the lithography is performed on the GaAs surface, an area is scanned and the plane is stored. Then the feedback loop is switched off during the lithography process. After the lithography has been performed, the feedback loop is activated and the same area is scanned again, revealing the anodized structure. The cantilever is exercised at its resonance frequency, and the vibrational amplitude is approximately 16–20 nm (peak to peak) during the scanning. During the regular scanning operation the tip–specimen distance (d) is approximately 10 nm, corresponding to the tapping and the total non-contact mode. A further description of the dynamic parameters needed to operate the AFM in a non-contact mode can be found elsewhere [13]. All the tests were performed three times and finally the averages of the three oxidation tests were taken and the error estimation was found to be approximately within 10–30%.

For environmental control, the microscope was placed in a closed box with inlets for dry and H_2O-saturated nitrogen. The relative humidity was controlled and ranged from 50–80% with an accuracy of 1% by a humidity regulator.

Further, to investigate the conversion of GaAs oxides, the chemical composition of the specimen was analysed by Auger electron spectroscopy (AES, Auger 670 PHI Xi, Physical Electronics, USA) system equipped with a Schottky field emission electron source.

Afterwards, the nanoindentation experiments were performed on these oxide structures using the AFM nanoindentation system equipped with a diamond tip (radius = 25 nm). The diamond tip was ground on three sides to yield an apex angle of 60°. The normal load was determined by multiplying the cantilever spring constant by the cantilever deflection. Nanoindentation tests were made in the load range of 12.8–76.5 μN with a cantilever stiffness of 255 N m^{-1}.

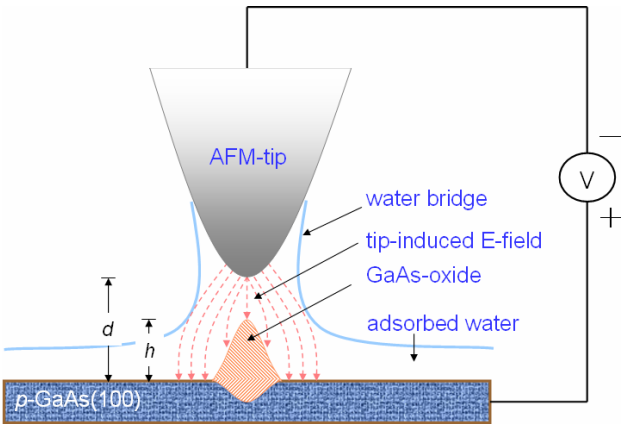

Figure 1. Schematic of the principle of AFM anodization. Here, d, h and d–h are the tip–specimen distance, the height of grown oxide and the separation between the top of the oxide dot and the AFM tip, respectively.

The indenter tip was used to image and locate an anodized GaAs-oxide structure and then *in situ* indent it with the same tip. Indents were performed on the anodized structures as a result of a normal load being applied on the surface by the tip. Nanohardness was calculated by dividing the indentation load by the projected residual area.

3. Results and discussion

For optimal AFM anodization processing of nanodevices, it is essential to understand the mechanisms and kinetics of the process so that the diagnostics can be reliably controlled. In figure 1, the principle of anodic oxidation on a p-GaAs(100) surface with an AFM tip is shown. In this technique, the AFM tip acts as a cathodically biased electrode to the specimen surface, while an adsorbed water layer on the specimen surface dissociates owing to a high electric field and acts as an electrolyte producing this electrochemical reaction. Oxyanions (OH^- and O^-) contribute to the formation of surface oxides and, owing to diffusion through the oxide layer, also to the growth of oxides underneath. This process strongly depends on the amount of adsorbed water and the water bridge size is increased as the anodized voltage or time increases. Further details of the size of the field-induced water bridge in nc-AFM can be found elsewhere [14, 15].

The oxide protrudes out of the GaAs surface because of the volume expansion owing to the incorporation of the oxygen atoms. As the oxide structures are formed, the positive voltage generates H^+ ions in the GaAs-oxide interface according to the electrochemical reaction [16]

$$2GaAs + 12h^+ + 10OH^- \rightarrow Ga_2O_3 + As_2O_3 + 4H_2O + 2H^+. \quad (1)$$

Here, h^+ denotes positively charged holes on the GaAs sample.

Figure 2 depicts a sequence of AFM imaged oxide dots fabricated using the nc-AFM based oxidation method. The patterns in figure 2(a) row 1 were obtained by using a constant voltage of 10 V at the different oxidation times of 10, 5, 2 and 1 s. The patterns in figure 2(a) row 2 were obtained by using a constant oxidation time of 5 s at the different anodization voltages of 7, 8, 9 and 10 V. These experiments were carried

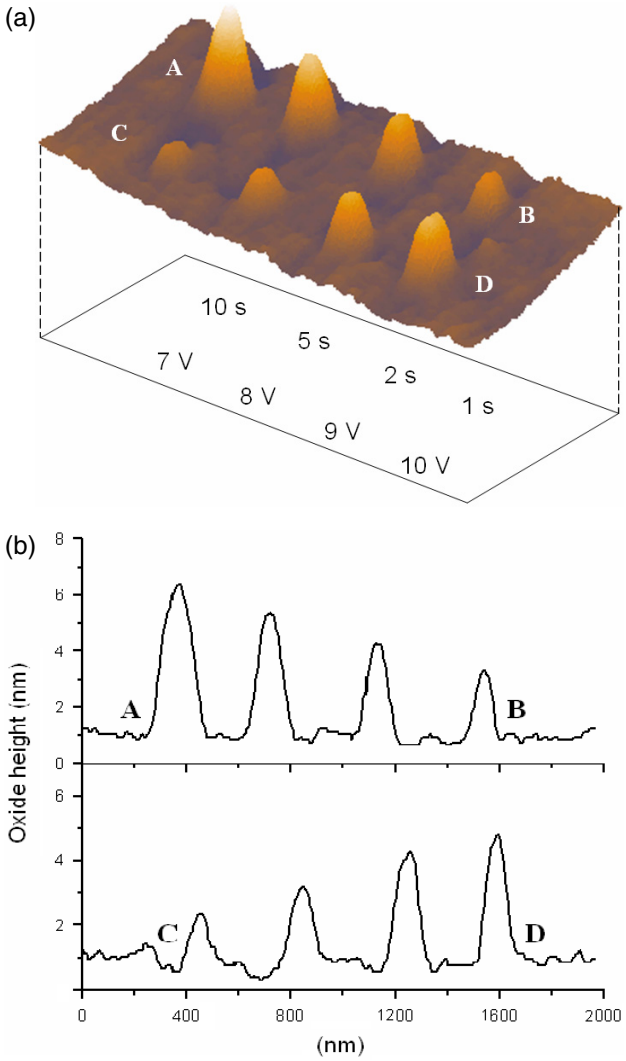

Figure 2. (*a*) An AFM image of nanodots on a *p*-GaAs(100) surface ($1000 \times 2000\,\mathrm{nm}^2$); (*b*) the height profiles of row 1 and row 2.

out in an environment having 60% relative humidity. The height profiles for the row 1 and the row 2 lines are shown in figure 2(*b*). It is found that a longer anodization time and a larger anodization voltage result in larger and higher oxidized dots. This implies that the oxide dots grow not only along the vertical direction but also along the horizontal direction. Figures 3(*a*) and (*b*) represent the oxide height, the aspect ratio and oxide volume as a function of the anodization time at the four anodization voltages mentioned previously. It can be seen that the oxide height, oxide volume and aspect ratio increase, as the logarithm of the anodization time increases and when the anodization voltage is increased. To pattern a dot for a given size the anodization times should be shorter or longer in relation to the corresponding anodization voltages which should be higher or lower, respectively. In the inset of figure 3(*a*), it is clear that the aspect ratio of *p*-GaAs(100) oxide could be improved using an anodized voltage, implying the enhancement of oxidation by the electric field.

The dependence of the oxide height, aspect ratio and oxide volume as a function of the anodization voltage at different various relative humidity levels is plotted in

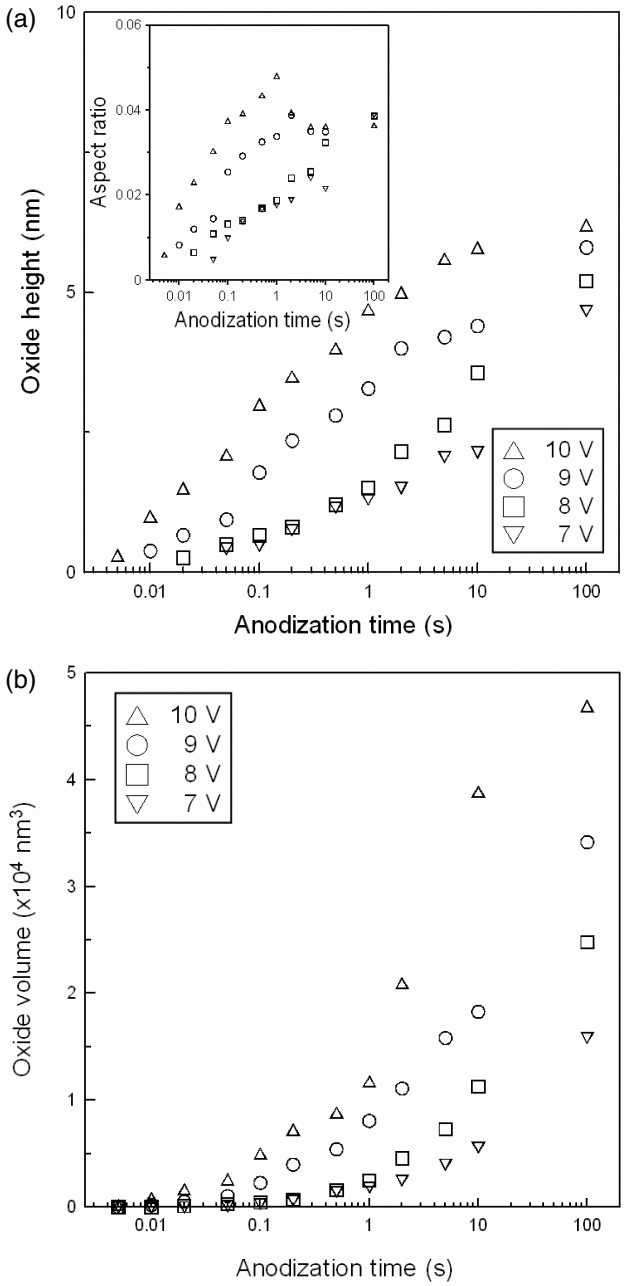

Figure 3. (*a*) Oxide height and aspect ratio as a function of the anodization times on different anodization voltages; (*b*) volume of the oxidized dots as a function of the anodization times at a relative humidity of 70%.

figures 4(*a*) and (*b*). It can be observed that the oxide height, oxide volume and aspect ratio increase as the relative humidity is increased, with the maximum size being formed at a relative humidity of 80%. From the inset of figure 4(*a*), there is no significant dependence of the aspect ratio on the humidity. The anodized oxide structure with a lower spatial resolution is obtained at a higher relative humidity, so that the resolution becomes worse as the relative humidity is increased [17].

In the case of optimizing the feature size, experiments were performed to determine the oxidation kinetics. In this paper, the curvature radius of the tip used in these experiments is about 3.5 times larger than *d* value; then the electrical

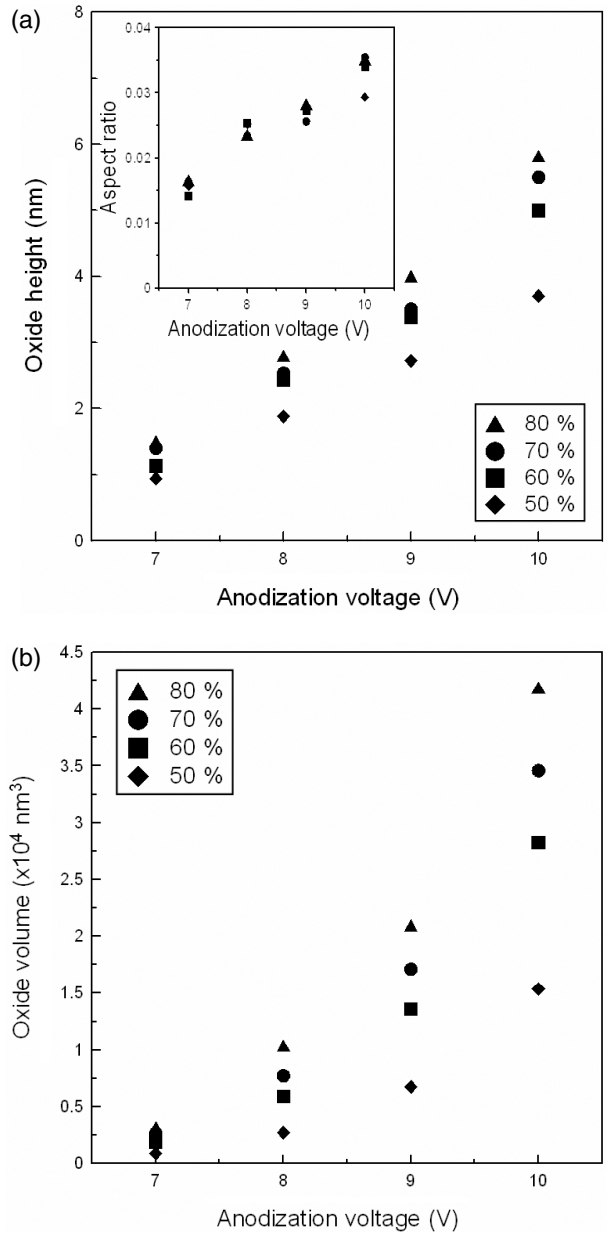

Figure 4. (*a*) Oxide height and the aspect ratio as a function of the anodization voltages on different relative humidity; (*b*) volume of the oxidized dots as a function of the anodization voltages at anodization time of 10 s.

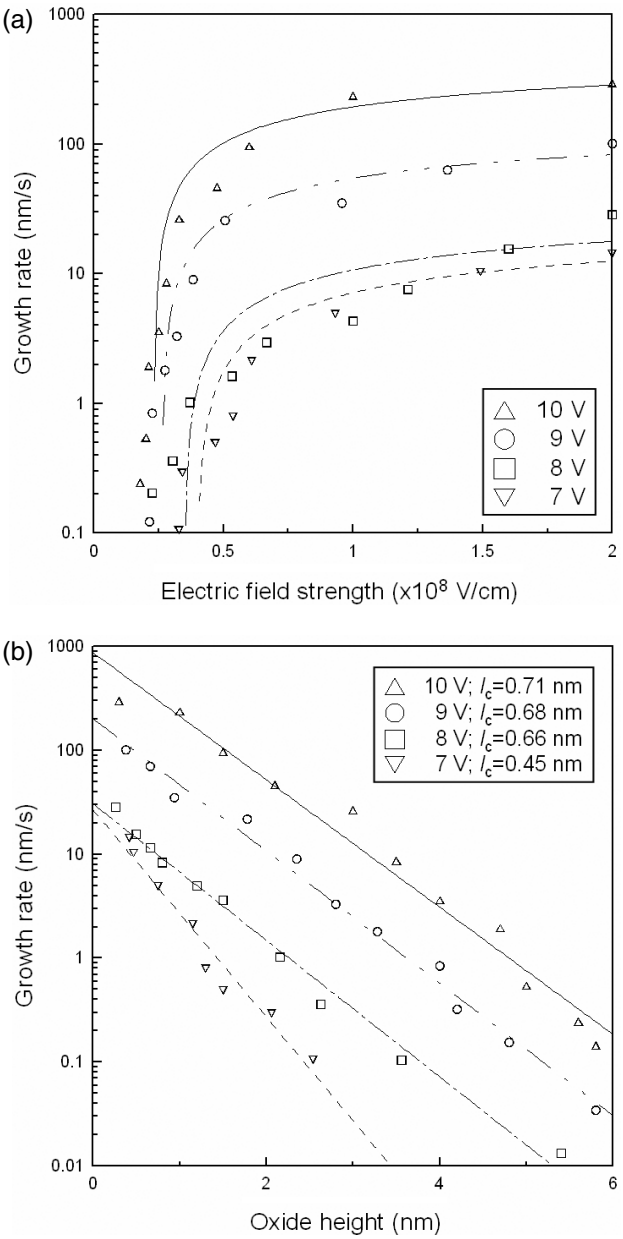

Figure 5. (*a*) Relationships of the growth rate and the electric field strength; (*b*) relationships of the growth rate and the oxide height.

field strength on the specimen surface and underneath the tip can be approximated by $E = V/h$ (with the constant anodic potential V, the strength of the field in oxide falls as anodic oxide is grown and, therefore, the electronic field is in inverse proportion to the height of the grown oxide, h). Oxide dots of different sizes were fabricated by the application of anodization voltages but at different anodization times. An estimation of the growth rate was obtained by calculating the ratio of the dot height to the time applied. As a consequence, the growth rate decreases exponentially with the height of the oxide (see figure 5(*b*)) and follows the equation as pointed out by Avouris *et al* [18]:

$$\frac{\mathrm{d}h}{\mathrm{d}t} \propto \exp\left(-\frac{h}{l_\mathrm{c}}\right), \tag{2}$$

where h is the oxide height at time t and l_c is a characteristic length dependent on the anodization voltage.

By advanced study of the oxidation kinetics, the patterned oxide dots are fabricated and analysed in figures 2(*a*) and 3(*a*) where clearly no threshold bias is observed. From figure 3(*a*), we can estimate the oxide height at which the electrochemical process is diffusion limited at ∼6 nm, and obtain the growth rate as a function of the electronic strength as shown in figure 5(*a*). Also in figure 5(*a*) it can be seen that the growth rate increases as the electric field strength and applied anodization voltages are increased. The initial growth rate is of the order of ∼300 nm s^{-1} for 10 V, but it decreases rapidly as the electric field strength is decreased. Additionally it is found that the anodization process is enhanced when the electric field strength is of the order of (2–3)×10^7 V cm^{-1}. It is also clear from figure 5(*a*) that the growth rate is not

only a function of electric field strength but also depends on the applied voltage. Moreover, figure 5(*b*) displays the relationships between the growth rate and the oxide height at four applied bias voltages. The characteristic decay length is within the range 0.45–0.71 nm at the applied anodization voltages of 7–10 V. Thus, as the oxide's height grows, the electric field becomes weaker and, accordingly, the growth rate decreases. Although, the applied anodization voltage is increased, the growth rate becomes faster and the characteristic length gets increased when the oxide's height reaches its maximum for each time.

As mentioned above, the applied tip bias extends the electric field strength assisting the oxidation mechanisms until the growth is limited by the diffusion. Not only is the oxide rate a function of electric field strength but it also appears to depend on the bias voltage applied to the tip. The Cabrera–Mott theory [19] of field-induced oxidation cannot account for this observed kinetics. The differences between the kinetics of AFM-induced oxidation and the Cabrera–Mott field model have been attributed to such mechanisms as: (1) the mechanical stress created and arisen within the oxide dots because of a large volume mismatch between the specimen and the oxide dots' structure [20] and (2) the space charge build-up within the oxide dots [21].

Previously [18] reported results on the development of the mechanical stress, arising during anodization, are due to a large volume mismatch in Si and SiO_2. The mechanical stress leads to additional activation energy, resulting in a rapid decrease in the growth rate while the oxide height increases rapidly. Similar results can also account for the AFM-induced oxidation in GaAs film [20], owing to the fact that the volume of $(Ga_2O_3 + As_2O_3)$ oxides is 2.7–3.5 times larger than that of GaAs and the SiO_2 oxides are 2 times larger than that of Si. Consequently, the mechanical stress of the oxides/GaAs interface is larger than the oxides/Si interface. An applied anodized voltage of 10 V causes the initial growth rate of the GaAs-oxide dot to be 300 nm s^{-1}, which is larger than the Si oxide dot that has a growth rate of 10 nm s^{-1} [18, 20]. In addition, the value of the growth rate of the AFM-generated oxide lines on *n*-GaAs(100) surface in [18] (about 50 nm s^{-1} at 10 V) is smaller than our results. If the applied bias voltages are the same, the faster the scan speed is performed the smaller the oxide structure that is obtained. This implies that the lower growth rate can be found in the oxide line structure. On the other hand, according to the report of Teuschler *et al* [22], the *p*-type Si(111) : H has higher oxide height than that of the *n*-type at a particular bias voltage as well as a higher growth rate. Thereby, we can speculate that the difference is reasonably explained by the differently doped substrates, oxide structures and operational conditions (such as AFM-operated mode and the humidity).

The nc-AFM local anodization was subjected to varying anodization voltages in the 7–10 V range; the diffusion limited electric field strength corresponding to the oxide height of ~6 nm is $(2–3)\times10^7$ V cm^{-1}. Thereby the AFM-based nano-oxidation process has a self-limiting behaviour resulting in a high initial oxidation rate, which decays exponentially, and reduces the electric field. The growth rate of the anodized film is governed by the ionic transportation that is promoted by the electric field strength. A greater height of the oxide protrusion corresponds to a weaker electrical field strength, which also limits oxide point growth. This model accounted for the self-limiting growth, which was proposed by Stiévenard *et al* [23]. The growth of the oxide structure is therefore fast in the initial stage of the anodization process, while there is a simultaneous rapid build-up of the space charge.

In 1993, Sugimura *et al* [24] proposed that the oxidation process is humidity dependent, leading to an interpretation of the process in terms of anodization, with the water acting as the electrolyte. Hence, the water bridge is very important because it plays the role of an essential component in the formation of the oxides. The relative humidity around the AFM tip and the specimen surface affects the oxides shapes as shown in the inset of figure 6 and, in previous studies [18, 25, 26]. At high relative humidity, the size and the shape of the oxide dots are changed obviously by virtue of the contribution of ion diffusion to the anodization process on *p*-Si(001) surface, as reported in [25]. Drawing inspiration from the previous studies, we also performed and discussed the process on *p*-GaAs(100) surface and found that the same phenomenon occurred at high relative humidity (over 60%) also.

Figure 6 shows the width of oxide dots patterned at different anodization times. It can be seen that the relative humidity dominates the lateral diffusion process as the anodization time progresses. Also, it has been proved that the water meniscus between the tip and the specimen surface is necessary for the SPM-based local oxidation and its size is dependent on the ambient humidity [27]. When the relative humidity was increased, a greater thickness of water meniscus formed around the tip–specimen junction (please see the inset of figure 6); also, the amount of oxyanions being migrated by an electric field in the lateral direction increased. That is, the water meniscus will become wider as the humidity increases and hence increase the quantity of OH^- ions contained within it, resulting in a significant enhancement of growth in the width of the induced oxides. At an anodized voltage of 10 V for 100 s, the anodized area broadened from 108 nm in width to 142 nm at the relative humidity of 50% and 80%, respectively. This process strongly depends on the amount of water available to be adsorbed, since the thicker is the water meniscus the higher is the humidity and, correspondingly, the specimen surface becomes anodized over a wider area [26, 27].

Further understanding of the nano-oxidation process can be obtained by measuring the Faradaic current [28], since the transport of oxyanions between the AFM tip and the specimen surface is ultimately responsible for the anodization process. High humidity promotes the contribution of ionic diffusion through surface water layer and decreases the Faradaic current. In terms of this, it can be concluded that the Faradaic current causes significant lateral ionic diffusion that produces a wider anodized area. Based on this point of view, we assume that a local diffusion coefficient of OH^- ion [29] in the solid–liquid interface is about $D = 10^{-9}$ cm^2 s^{-1} and the average displacement travelled by an ion is given by $r \sim \sqrt{Dt}$. In our case for $t = 0.01$ s, $r \sim 32$ nm is approximately the experimental width value. However, the experimental width value cannot be expected to grow with the theoretical value of ~3200 nm at 100 s because of the space charge build-up which arrested the lateral growth behaviour. As revealed in figure 5(*a*), the anodization process is limited as a result of

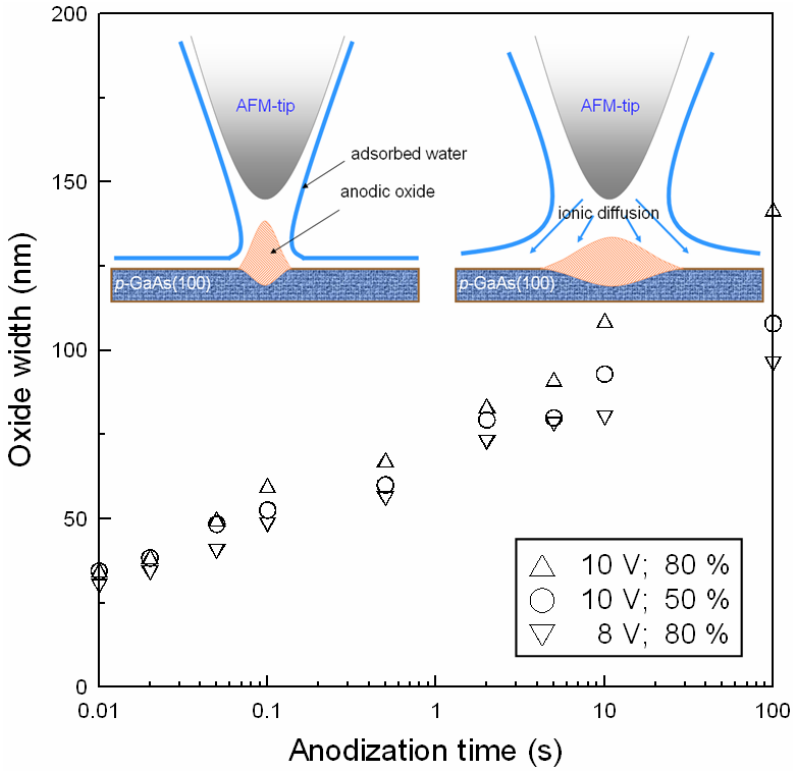

Figure 6. Relationships of the oxide width and the anodization time. The inset illustrates the low and the high humidity conditions.

the space charge accumulation at oxides/GaAs interface, as described earlier.

As per the above analysis, the change in the oxide volume is obviously greater at the higher anodization voltage and the relative humidity at longer anodization time, and this implies that the continuation of oxidation is due to the contribution of ionic diffusion [25]. The contribution of ionic diffusion [25] to the AFM anodization process and an oxide dot with a 'two-storied' shape (the parts of narrow upper and broad base) are illustrated in figure 7, which are caused by the space charge effect and lateral ionic diffusion. At longer anodization times, the ion diffusion at 8 V goes up to about 70% and at 10 V goes up to about 80% while it remains below 30% when the anodization time is shorter even though the relative humidity is higher. The ion diffusion phenomenon thus occurs at a longer anodization time and a higher anodized voltage. When comparing the contribution of ionic diffusion between GaAs and Si, it was found that GaAs had a higher contribution of ionic diffusion than Si owing to a higher growth rate.

The electrochemical reaction causes local oxidation at the p-GaAs(100) surface, that is, the electrical field drives OH^- ions in the water bridge to GaAs surface resulting in the formation of the oxides. To provide proof of that, AES analysis was conducted on an anodized area of $10 \times 10\,\mu m^2$. This region was created by nc-AFM operated at a scanning speed of $1\,\mu m\,s^{-1}$ at an applied voltage of +10 V. In figures 8(a) and (b), AES records taken from the as-grown and modified areas are illustrated. Both spectra have emission peaks of Ga–*LMM* at ∼1065 eV and As–*LMM* at ∼1225 eV. Obviously, we can see the emission peak of O–*KLL* Auger electrons having the kinetic energy of ∼512 eV in figure 8(b). Meanwhile, the magnitude of O–*KLL* is much enhanced on the anodized region as compared with that of the as-grown region, which suggests higher oxygen content in the modified area. The AES results support the suggestion of the previous study that the heavily C-doped GaAs film can be converted to oxides by local oxidation process [30]—the mobile oxyanions drift towards the anodic specimen in response to the local electrical field beneath an AFM tip and react with p-GaAs(100) surface at the oxides/GaAs interface. In addition, x-ray photoelectron spectroscopy (XPS) is a powerful technique for analysing surface chemistry and composition. In the previous study [31], the chemical analysis of AFM tip-induced n^+-GaAs(100) oxide had also revealed that the main constituents are determined to be Ga_2O_3 and As_2O_3 by means of scanning microprobe XPS measurements. As a result of AES and XPS analyses, the products are shown to be GaAs oxides in a qualitative analysis briefly.

In closing, AFM tip-induced nano-oxidation process is dependent on the electric field and the relative humidity. As the relative humidity increases, the spatial extent of the water meniscus also increases, which influences the process along with the applied bias voltage [25] because it determines the amount of adsorbed water layer and the primary source of oxyanions in the electrochemical reaction. Oxyanions are produced by the hydrolysis of the water within the meniscus. Such ions transport across the anodic oxide is strongly accelerated by an intense electric field produced in the oxide by the applied bias voltage. In this electrochemical reaction, the high electrical field of the AFM tip produces oxyanions in the relative humidity that forms Ga(As)–O bonds on the surface.

Furthermore, the purpose of this part is to evaluate some of the mechanisms and the kinetics of p-GaAs(100) by AFM-based surface oxidation process. First, the growth

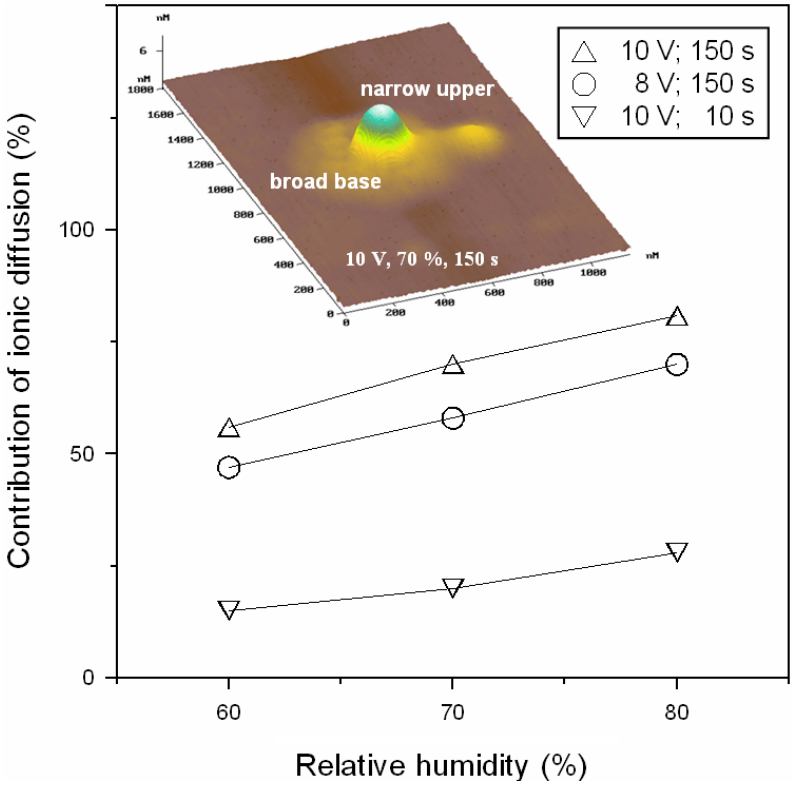

Figure 7. The contribution of ionic diffusion to anodized dots and the inset shows a 'two-storied' anodized shape dot with the broad base and the narrow upper parts.

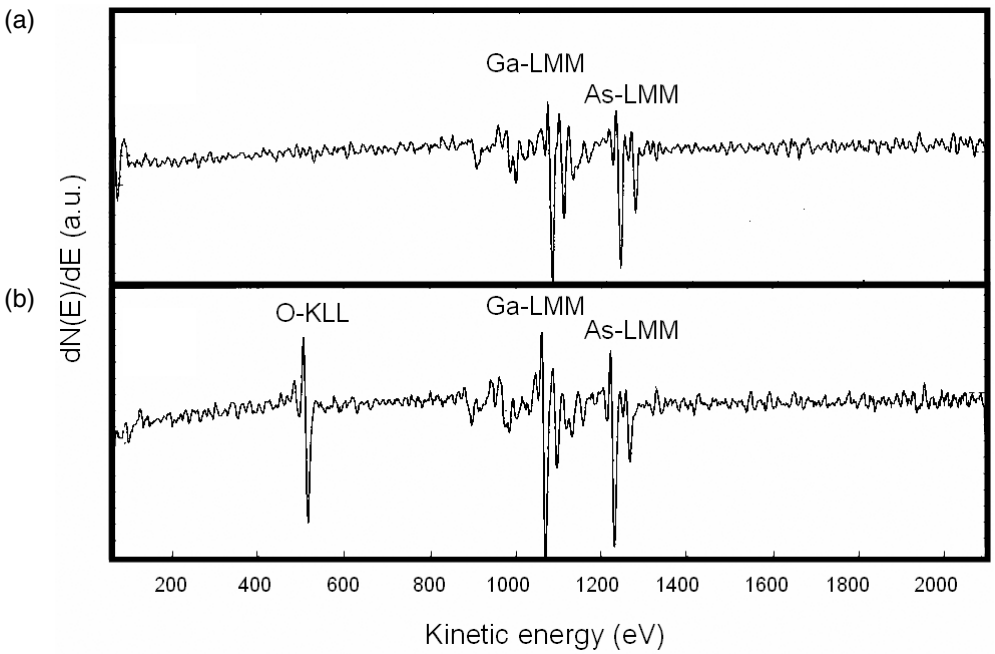

Figure 8. AES spectra of (*a*) the as-grown and (*b*) the anodized oxide areas on *p*-GaAs(100) surface.

norm must be the same in both phenomena, since it is limited only by electric-field-simulated ionic diffusion into the oxide structures. Thus, it is expected that there exists a mechanism to reduce the electric field strength within the oxide dots. For such a mechanism, an increase in the H^+ ion concentration near the oxide layer during the anodization processes has been considered [32]. As the anodization time progresses, the H^+ concentration in the oxide grows and becomes significant. As a result of the screening effect of the H^+ ions, there is a decrease in the electric field within the

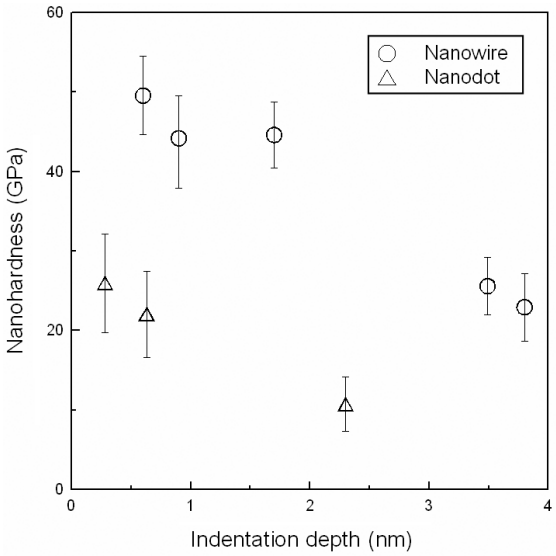

Figure 9. Nanohardness as a function of indentation depth for the anodized structures.

oxide dots and this may be the reason for the lower oxidation. Second, as revealed by AES analysis, it suggests that the incorporation of oxygen into p-GaAs(100) surface is enhanced because AFM nano-oxidation process results in the formation of anodized oxides.

If these GaAs-oxide structures are used at very light loads such as effect tunnel barriers for carrier transport in device applications, the high hardness of anodized nanostructure would protect the device until it is worn out. Therefore, the mechanical property of the anodized oxides should be recognized.

The nanohardness of the anodized nanowires and the nanodots as a function of indentation depth are shown in figure 9. The nanohardness does not show any change as the indentation depth is increased up to ∼2 nm. The nanohardness of the anodized nanowire at the shallowest indentation depth of 0.6 nm was 49.5 GPa and it dropped to a value of 22.9 GPa at an indentation depth of 3.8 nm. The nanohardness of the anodized nanodot at the shallowest indentation depth of 0.3 nm is 25.9 GPa and it drops to a value of 10.8 GPa at an indentation depth of 2.3 nm. Table 1 shows the data available for the mechanical properties of Si, SiO_2, GaAs and tip-induced GaAs oxides. As can be noted, the AFM tip-induced GaAs oxides exhibit larger hardness values than other semiconductor materials, with the possible deduction that they exhibit the larger internal stress. This is because large stress is being built up owing to the volume mismatch between the GaAs-oxides and the surrounding non-anodized GaAs during the AFM anodization processes. Of note, the nanohardness of the anodized nanowires is about 2 times higher than that of the anodized nanodot. From a microscopic view it can be deduced that the cause could be the influence of plastic deformation or different geometrical restrictions. The nanohardness behaviour at indentation depths greater than 2 nm can be explained by the plastic deformation occurring because of the contact between the structure and the AFM probe tip. The nanohardness drops at indentation depths greater than 2 nm owing to the substrate influence and the indentation size effect, as mentioned by Bhushan and Li [36] and Nix and Gao [37].

Table 1. Values of the hardness obtained in this work compared with what was previously reported for the semiconductors studied.

Materials	Hardness (GPa)
Si(110)	12 [33]
SiO_2	8.3 [34]
GaAs(001)	6.7–7 [35]
p-GaAs(100)	9.5–10.8[a]
Tip-induced p-GaAs(100)oxide	Dot: 10.8–25.9[a]
	Wire: 22.9–49.5[a]

[a] This paper.

4. Conclusion

The combination of AFM-based nano-oxidation and nanoindentation techniques has been used to investigate the anodized nanostructures on a p-GaAs(100) surface.

The AFM anodization process has taken place at the oxides/GaAs interface, enhanced by a tip–specimen electric field in the presence of humidity and its electrochemical characteristics have displayed the importance of the mechanisms of the space charge and the ionic diffusion. The results indicate that larger and higher oxide protrusions as well as a higher aspect ratio were produced at longer anodization times, higher anodization voltages and at higher relative humidity. The anodization process is enhanced when the electric field strength is of the order of $(2–3)\times10^7$ V cm^{-1}. The growth rate decreases, which can be attributed to the reduction in the electric field strength when the oxide height increases. The analysis of the nanodot's height and volume at various anodized voltages indicates that the growth of nanodots is limited by the field-enhanced diffusion mechanisms of OH^- ions through the oxides. At a relative humidity of 70% a two-storied shape nanodot caused by the ionic diffusion was found. The evidence of the oxides growth on GaAs surface owing to AFM tip-induced oxidation was

confirmed by AES analysis. The nanohardness of the anodized nanowires and the nanodots is in the range of 22.9–49.5 GPa and 10.8–25.9 GPa, respectively. Results carried out on specimens of anodized nanowires and nanodots show that an ISE on the mechanical properties becomes significant at a threshold point as the indentation depth is of 2 nm.

Acknowledgment

This work was partially supported by the National Science Council of Taiwan, under Grant No NSC93-2218-E218-005 and NSC94-M2120-009-002.

References

[1] Dagata J A, Schneir J, Harary H H, Evans C J, Postek M T and Bennett J 1990 *Appl. Phys. Lett.* **56** 2001
[2] Matsumoto K, Ishii M, Segawa K, Oka Y, Vartanian B J and Harris J S 1996 *Appl. Phys. Lett.* **68** 34
[3] Shingubara S, Murakami Y, Morimoto K and Takahagi T 2003 *Surf. Sci.* **532/535** 317
[4] Tsau L, Wang D and Wang K L 1994 *Appl. Phys. Lett.* **64** 2133
[5] Ishii M and Matsumoto K 1995 *Japan. J. Appl. Phys.* **34** 1329
[6] Sasa S, Ikeda T, Dohno C and Inoue M 1998 *Physica* E **2** 858
[7] Day H C and Allee D R 1993 *Appl. Phys. Lett.* **62** 2691
[8] Irmer B, Kehrle M, Lorenz H and Kotthaus J P 1997 *Appl. Phys. Lett.* **71** 1733
[9] García R, Calleja M and Pérez-Murano F 1998 *Appl. Phys. Lett.* **72** 2295
[10] Martin Y, Williams C C and Wickramasinghe H K 1987 *J. Appl. Phys.* **61** 4723
[11] Dubois E and Bubbendoroff J L 1999 *Solid-State Electron.* **43** 1085
[12] Tello M and García R 2001 *Appl. Phys. Lett.* **79** 424
[13] García R and Paulo A S 1999*Phys. Rev.* B **60** 4961
García R and Paulo A S 2000 *Phys. Rev.* B **61** R13381
Paulo A S and García R 2002 *Phys. Rev.* B **66** 041406
[14] Gómez-Moñivas S, Sáenz J J, Calleja M and García R 2003 *Phys. Rev. Lett.* **91** 056101
[15] Calleja M, Tello M and García R 2002 *J. Appl. Phys.* **92** 5539
[16] Ghandhi S K 1994 *VLSI Fabrication Principle* (New York: Wiley)
[17] Sugimura H, Yamamoto T, Nakagiri N, Miyashita M and Onuki T 1994 *Appl. Phys. Lett.* **65** 1569
[18] Avouris P, Hertel T and Martel R 1997 *Appl. Phys. Lett.* **71** 285
[19] Cabrera N and Mott N F 1949 *Rep. Prog. Phys.* **12** 163
[20] Okada Y, Amano S, Kawabe M and Harris J S Jr 1998 *J. Appl. Phys.* **83** 7998
[21] Dagata J A, Inoue T, Itoh J, Matsumoto K and Yokoyama H 1998 *J. Appl. Phys.* **84** 6891
[22] Teuschler T, Mahr K, Miyazaki S, Hundhausen M and Ley L 1995 *Appl. Phys. Lett.* **67** 3144
[23] Stiévenard D, Fontaine P A and Dubois E 1997 *Appl. Phys. Lett.* **70** 3272
[24] Sugimura H, Uchida T, Kitamura N and Masuhara H 1993 *Appl. Phys. Lett.* **63** 1288
[25] Kuramochi H, Ando K and Yokoyama H 2003 *Surf. Sci.* **542** 56
[26] Jungblut H, Wille D and Lewerenz H J 2001 *Appl. Phys. Lett.* **78** 168
[27] Sugimura H, Uchida T, Kitamura N and Masuhara H 1994 *J. Phys. Chem.* **98** 4352
[28] Kuramochi H, Ando K and Yokoyama H 2003 *Japan. J. Appl. Phys.* **42** 5892
[29] Lide D R (ed) 1994 *CRC Handbook of Chemistry and Physics* (Boca Raton, FL: CRC Press)
[30] Shirakashi J I, Matsumoto K and Konagai M 1998 *Appl. Phys.* A **66** S1083
[31] Okada Y, Iuchi Y, Kawabe M and Harris J S Jr 1998 *J. Appl. Phys.* **88** 1136
[32] Dagata J A, Inoue T, Itoh J and Yokoyama H 1998 *Appl. Phys. Lett.* **73** 271
[33] Pharr G M, Oliver W C, Cook R F, Kichner P D, Kroll M C, Dinger T R and Clarke D R 1992 *J. Mater. Res.* **7** 961
[34] Pethica J B, Hutchings R and Oliver W C 1983 *Phil. Mag.* A **48** 593
[35] Trifonanva E P and Hitova L 1993 *Thin Solid Films* **224** 153
[36] Bhushan B and Li X 2003 *Int. Mater. Rev.* **48** 125
[37] Nix W D and Gao H 1998 *J. Mech. Phys. Solids* **46** 411